New bleeding model of additives in a polypropylene film under atmospheric pressure II

doi: 10.1002/app.26723

Manuscript

A new bleeding model of additives in a polypropylene film under atmospheric pressure II

***M.Wakabayashi, T.Kohno, T.Kimura, S.Tamura, M.Endoh, S.Ohnishi, T.Nishioka, Y.Tanaka, T.Kanai**

Theme

A new bleeding model of additives in a polypropylene film under atmospheric pressure II

Author

*Makoto Wakabayashi[(a,b)], Takayuki Kohno[(c),] Tokutaro Kimura[(c)], Satoshi Tamura[(c),], Masahiko Endoh[(c)], Satoru Ohnishi[(d)], Toshikatsu Nishioka, Yoshikatsu Tanaka[(c)] , Toshitaka Kanai[(a,b)]

(a)Idemitsu Kosan Co., Ltd., Ichihara, Chiba 299-0193, Japan
(b)Graduate School of Natural Science and Technology, Kanazawa University, Kanazawa, Ishikawa 920-1192, Japan
(c)Prime Polymer Co., Ltd., Sodegaura, Chiba 299-0265, Japan
(d)Idemitsu Unitech Co., Ltd., Sodegaura, Chiba 299-0205, Japan

[*]Mail address:
Makoto Wakabayashi,
Central Research Laboratories, Idemitsu Kosan Co., Ltd.
1-1, Anesaki-Kaigan, Ichihara, Chiba, 299-0193, JAPAN
E-mail: makoto.wakabayashi @si.idemitsu.co.jp

ABSTRACT:

Many additives are commercially used to add more favorable qualities to films. The bleeding process by which the additive in a film comes to the surface is considered. A new bleeding model of additives in a polypropylene film under atmospheric pressure was investigated. Solubility and diffusion are found to be important for explaining this bleeding process. It was found that the experimental results were explained more precisely by assuming a two step transport process between the crystalline regions and the amorphous ones. The solubilities and diffusion coefficients of UV-stabilizers such as 2-(2H-Benzotriazol-2-yl)-4-(1,1,3,3-tetramethylbutyl)phenol and 2-(2H-Benzotriazol-2-yl)-4-methylphenol were determined at 40°C. The difference between the saturation solubilities and the diffusion coefficients of UV-stabilizers was discussed by comparing with the results of molecular dynamics (MD) simulation.

Keywords: Polypropylene; Films; Additives; Solubility; Diffusion

INTRODUCTION

Many additives are used to add more favorable qualities to films. There are some additives which provide performance by bleeding on the surface of the film such as a slip agent or an anti-static additive, etc. Also, there are other additives applied inside the film, for example an UV-stabilizer and antioxidant, etc. The bleeding process by which the additive in a film comes to the surface will be considered to be effective in design development of additive prescription, if it can be predicted.

There are many reports regarding the solubilities and the diffusions of additives in polymer films[1-11]. To measure the diffusion coefficient and the solubility, the methods of using the permeation through a film, adsorption in a film and release from a film have been devised[12-15]. It is reported that the bleeding process can be explained by the solubility and the migration speed of an additive in a film. However, it is thought that the diffusion is influenced by the different morphology such as a crystalline state and an amorphous state.

Quijada-Garrido and others reported the migration speed of the erucamide (13-cis-docosenamide) in an isotactic-polypropylene (iPP) film under atmospheric pressure and vacuum.[16,17]. In the previous paper[18,19], it was shown that the bleeding process of slip agents under atmospheric pressure were explained more precisely by assuming a two step transport process between the crystalline regions and the amorphous ones. In this paper, the two step transport model was applied to the bleeding process of UV-stabilizers under atmospheric pressure. The difference between the diffusion coefficients and the saturation solubility of UV-stabilizers was discussed by using the molecular dynamics (MD) simulation.

EXPERIMENTAL

Materials

Idemitsu H700 additive-free isotactic polypropylene (iPP) was used. It has a nominal density of 900 kg/m^3, MFR 7.0 g/10min, 47% of crystallinity, 93.2mol% of isotactic pentad fraction evaluated by ^{13}C NMR spectroscopy and average molecular masses of H700 are $M_n = 4.87 \times 10^4$, $M_w = 3.25 \times 10^5$ and $M_z = 1.31 \times 10^6$ estimated by size exclusion chromatography. 2-(2H-Benzotriazol-2-yl)-4-(1,1,3,3-tetramethylbutyl)phenol (UVA-1, Tinuvin 329) and 2-(2H-Benzotriazol-2-yl)-4-methylphenol (UVA-2, Tinuvin P) were supplied by Ciba-Geigy.

Sample preparation and measurements

The blends of iPP/UVA-1 or iPP/UVA-2 with a small quantity of antioxidant additives (500ppm of IRGANOX 1076 (Ciba-Geigy) and 500ppm of IRGAFOS 168 (Ciba-Geigy)) were prepared by dry mixing and then fed into single-screw extruder operated at 200°C with a screw speed of 100rpm. They were quenched in cold water and cut into the pellet form. The obtained pellets were fabricated into 60 μm film in thickness using the Φ 40mm T-die casting machine where the temperature from the bottom of the hopper to the T-die was set from 200°C to 230°C with a screw speed of 80rpm. The film was chilled at 30°C. Several sets of 50 sheets of film whose area became 100cm^2 (10cm long and 10cm wide) were prepared and were put in the oven quickly after fabrication for bleeding under the predetermined time at 40°C.

A set of the 50 sheets of film was taken out from the oven after predetermined time. Each surface of 50 sheets of film was put in 500ml acetone for 5 seconds and then washed for 5 seconds. The solvents were eliminated by using rotary evaporator. The dried residuals were dissolved in tetrahydrofuran with no stabilizer (about 0.2w/v%). The amounts of the UV-stabilizers were determined by size exclusion chromatography with a Waters 410 RI detector at 40°C and tetrahydrofuran with no stabilizer as eluent.

RESULTS AND DISCUSSION

Two step transport model

In the previous paper[18], the optimal model for describing the bleeding process under atmospheric pressure was reported. The bleeding process in the amorphous state is thought to be governed by Fick's equations (1) with the appropriate boundary conditions.

$$\frac{\partial c}{\partial t} = D\frac{\partial^2 c}{\partial x^2} \qquad (1)$$

where c is the concentration of diffusion material in any point x at time t, and D is the diffusion coefficient. The boundary conditions of Fick's equation, which assumed the diffusion in the object spread infinitely, were examined. The boundary conditions of this diffusion model are described below.

$$\begin{aligned} t = 0 \quad & c = C_{0,i} - C_s \quad && (-l < x < l) \\ & c = 0 && (x < -l,\ l < x) \end{aligned} \qquad (2)$$

where l is the half thickness of the film, $C_{0,i}$ is the ith initial amount of an additive and C_s is the saturation solubility. The solution yields this expression

$$C(x,t) = \frac{C_{0,i} - C_s}{2} c(x,t) \tag{3}$$

$$c(x,t) = erf\left(\frac{l-x}{2\sqrt{Dt}}\right) + erf\left(\frac{l+x}{2\sqrt{Dt}}\right) \tag{4}$$

where $erf(x)$ is the error function described below.

$$erf(x) = \frac{1}{\sqrt{\pi}} \int_0^x \exp(-t^2) dt \tag{5}$$

Then the amount of bleeding additive on the film $y(t)$ is assumed to be the difference between the excess amount of additive ($C_{0,i}$-C_s) and the remaining amount of additive inside the film at time t.

$$y(t) = \left(C_{0,i} - C_s\right)\left(1 - \frac{1}{4l}\left(\int_{-l}^{l} c(x,t) dx\right)\right) \tag{6}$$

Figure 1 shows the concept for calculation of the bleeding process. The area outside of the film surface is assumed to be the amount of bleeding additive.

We considered the bleeding process of the additives under atmospheric pressure as follows. The additive in an iPP film dissolves in an amorphous region first, and if it reaches saturation solubility it becomes impossible to dissolve more. The ingredient beyond this saturation solubility migrates to the film surface at a certain speed according to the diffusion process. Furthermore as shown in Figure 2, it is known that an iPP film has spherulites (S) and amorphous regions (A), which are supposed to have a different contribution to the migration speed in the bleeding process. The spherulites have folded crystalline regions (C) and the additives exist among the crystalline regions (A'). So the model had to be modified in consideration of the amorphous regions and the crystalline regions. We considered that a portion of the excess amount beyond the saturation solubility was restricted within crystalline regions in the spherulites and migrated slowly according to the first-order kinetics. The rest of the excess amount of

additives which is not restricted in the crystalline regions exists in the amorphous regions among spherulites. The extent of restriction within crystalline regions was assumed to increase according to the initial amount of the additives. So two step transport model yields the expression

$$y(t) = \left(C_{0,i} - C_s\right)\left\{\alpha_i + \left(1-\alpha_i\right)\left(1-\exp\left(-kt\right)\right)\right\}\left(1 - \frac{1}{4l}\left(\int_{-l}^{l} c(x,t)dx\right)\right) \qquad (7)$$

$$c(x,t) = erf\left(\frac{l-x}{2\sqrt{Dt}}\right) + erf\left(\frac{l+x}{2\sqrt{Dt}}\right) \qquad (8)$$

where $y(t)$ is the amount of bleeding additive on the film surface at time t, $C_{0,i}$ is the ith initial amount of an additive, C_s is the saturation solubility, α_i is a diffusion ratio of the initial amount $C_{0,i}$, k is the constant of first-order kinetics, l is the half thickness of film, $c(x,t)$ is the concentration at time t and distance x, $erf(x)$ is the error function and D is the diffusion coefficient.

The diffusion ratio α_i is assumed to be larger at a lower concentration of additive, because the restriction within the crystalline regions of spherulites is thought to be weak at a lower concentration. Values of α_i, D and C_s are calculated by the least squares technique using a computer program of the best fitting between the experimental data and equations (7) and (8).

The results of UVA-1 and UVA-2 at 40ºC calculated using the two step transport model is shown in Figure 3 and 4 respectively. When the initial amount of UVA-2 was 2700ppm, there was no bleed on the film surface because the initial amount was less than the saturation solubility. The two step transport model explains the bleeding profiles of UVA-1 and UVA-2 well. TABLE I summarizes the saturation solubilities, the diffusion coefficients, the constants of first-order kinetics and the diffusion ratios based on the two step transport model. The values of saturation solubility (C_s) of UVA-1 and UVA-2 were calculated with 13,000ppm and 3000ppm respectively. On the other hand, the values of the diffusion coefficient (D) of UVA-1 and UVA-2 were calculated with 2.4×10^{-14} m^2/s and 7.4×10^{-14} m^2/s respectively. There are big differences to the values of saturation solubility and the diffusion coefficient about UVA-1 and UVA-2. The value of the diffusion ratio (α_i) of UVA-1 is zero, but that of UVA-2 is 0.11 obtained from this experiment. The diffusion ratio of UVA-1 is smaller than that of UVA-2. It is thought that the almost all molecules of UVA-1 are restricted in the spherulites. On the other

hand, the molecules of UVA-2 are slightly free from the restriction of spherulites. In order to study the cause in which UV-stabilizers with the almost same structures have a big difference in bleeding process, the important factors C_s and D were examined using molecular dynamics (MD).

Estimation of solubility parameter by molecular dynamics (MD)

The Hildebrand solubility parameter (δ) is defined as the square root of cohesive energy density

$$\delta = \sqrt{\frac{E_{coh}}{V}} = \sqrt{\frac{E_{vac} - E_{bulk}}{V}} \qquad (9)$$

where E_{coh} is the cohesive energy per mole, E_{vac} is the potential energy in the vacuum state, E_{bulk} is the potential energy in the bulk state and V is the mole volume. The values of E_{vac}, E_{bulk} and V were calculated from MD simulation. The MD simulations were performed using commercial package, NanoBox software from Nano Simulation Associates, Japan[20-22]. By using the united atom (UA) model under NPT condition[23,24], the temperature was fixed by the Nose-Hoover method[25,26] and the pressure was controlled by Andersen's method[27]. The electrostatic interactions were computed using the spherical Ewald truncation method[28].

The potential energies and the mole volumes of the bulk state were calculated as follows. Fifty molecules of UVA-1 or fifty molecules of UVA-2 were prepared in one unit cell. The bulk amorphous states were built using cubic unit cell subjected to periodic boundary conditions. The system was compressed by performing 50ps duration using a time step of 2fs under 10 MPa at 473K. Then the system was equilibrated by performing 500ps duration using a time step of 2fs under 0.1MPa at 313K. The main runs were performed 500ps duration using a time step of 2fs under 0.1MPa at 313K. The potential energies in the vacuum state were calculated as follows. The last unit structure of the bulk state calculation was expanded uniformly so that the molecular structures might not change where the cell-edge lengths of x, y and z-axes were set as 100nm respectively. Then the potential energy of this expanded unit structure was calculated.

Figure 5 and 6 show the conformations of UVA-1 and UVA-2 after main run respectively. As shown in TABLE II, the solubility parameters of UVA-1 and UVA-2

obtained by MD calculation are 19.3, 22.7 respectively. As compared with these solubility parameters, the solubility parameter of UVA-1 is closer to that of PP. This result is consistent with the fact that the saturation solubility of UVA-1 becomes larger than that of UVA-2. It is supposed that the solubility parameter influences the saturation solubility because of the different compatibility of the functional group.

Estimation of diffusion coefficient by molecular dynamics (MD)

The values of the diffusion coefficients obtained by this two step transport model were compared with the result of MD simulation. Five polymer chains of the 1200 degrees of polymerization which had the almost same molecular mass (50,000) as iPP used in this paper were prepared. Nine molecules of UVA-1 and three molecules of UVA-2 were added with iPP in a unit cell respectively so that it might become the almost same amounts which is in agreement with the saturation solubility. The bulk amorphous state of the blends were built using cubic unit cells subjected to periodic boundary conditions. The system was compressed by performing 50ps duration using a time step of 2fs under 10 MPa at 473K. Then the system was equilibrated by performing 1500ps duration using a time step of 2fs under 0.1MPa at 313K. The main runs were performed 500ps duration twice using a time step of 2fs under 0.1MPa at 313K. Figure 7 shows the typical conformation of iPP/UVA-1 blends with five chains of iPP and nine molecules of UVA-1 after main run. Figure 8 also shows the typical conformation of iPP/UVA-2 blends of five chains of iPP and three molecules of UVA-2 after main run. As shown in TABLE III, both densities were consistent with each other.

The self diffusion coefficients (D_{self}) were calculated using the equation below

$$D_{self} = \lim_{t\to\infty} \frac{1}{6t} \left\langle \left| \mathbf{r}(t+t_0) - \mathbf{r}(t_0) \right|^2 \right\rangle \qquad (10)$$

where $\left\langle \left| \mathbf{r}(t+t_0) - \mathbf{r}(t_0) \right|^2 \right\rangle$ is the averaged mean square distribution, $\mathbf{r}(t)$ is the center of gravity of the additive. The values of D_{self} were calculated using data from 60ps to 200ps.

Figure 9 shows the time dependency of the mean square distribution of UVA-1 and UVA-2. TABLE III and Figure 10 shows the comparison between the self diffusion coefficients calculated from MD and the diffusion coefficients obtained from the two

step transport model. There are good relationship between the diffusion coefficients from MD and the two step transport model. Since UVA-1 has a large functional group (tert-octyl group), it is thought that the diffusion coefficient of UVA-1 is smaller than that of UVA-2. The values of the self diffusion coefficients of both UV-stabilizers from MD are quite smaller than the value of methane ($0.7\text{-}1.3 \times 10^{-10} m^2/s$) [24], however these values are still about 100 times as large as the diffusion coefficients obtained from the two step transport model. The calculated values from MD present the self diffusion coefficients of additives of Brownian motion in the very narrow range (about 2Å) of the amorphous state. On the other hand, the calculated values from the two step transport model present relative diffusion coefficients of UV-stabilizers which are thought to be restricted by the various barriers when the additives pass from the crystalline regions to the amorphous regions among the spherulites and pass through the amorphous regions among the spherulites to the film surface as shown in Figure 2.

It is demonstrated that the MD simulation is useful for predicting the saturation solubilities and the diffusion coefficients of UV-stabilizers qualitatively in spite of the large molecular sizes and complex structures of iPP film.

CONCLUSIONS

A new bleeding model of additives in an isotactic polypropylene film under atmospheric pressure was investigated. The two step transport model explains the bleeding profiles of UV-stabilizers such as 2-(2H-Benzotriazol-2-yl)-4-(1,1,3,3-tetramethylbutyl)phenol and 2-(2H-Benzotriazol-2-yl)-4-methylphenol well. By using this model, the saturation solubilities and diffusion coefficients of the UV-stabilizers were directly determined at 40°C. By using MD simulation, the Hildebrand solubility parameter is supposed to influence the saturation solubility because of the different compatibility of the functional group. The size of the functional group is also supposed to influence the diffusion coefficient. MD simulation is useful for predicting the saturation solubilities and the diffusion coefficients qualitatively in spite of the large molecular sizes and complex structures of iPP film.

Acknowledgments

The authors would like to thank Mr. Norio Senda for use of the 3-dimensional computer graphics of Winmostar.

References

1. Billingham, N. C.; Calvert, P. D.; Manke, A. S. J Appl Polym Sci 1981, 26, 3543.
2. Földes, E.; Turcsányi, B. J Appl Polym Sci 1992, 46, 507.
3. Földes, E. J Appl Polym Sci 1993, 48, 1905.
4. Földes, E. J Appl Polym Sci 1994, 51, 1581.
5. Möller, K.; Gevert, T. J Appl Polym Sci 1994, 51, 895.
6. Spatafore, R.; Pearson, L. T. Polym Eng Sci 1991, 31, 1610.
7. Schwarz, T.; Steiner, G.; Koppelmann, J. J Appl Polym Sci 1989, 37, 3335.
8. Koszinowski, J. J Appl Polym Sci 1986, 31, 2711.
9. Hayashi, H.; Sakai, H.; Matsuyama, S. J Appl Polym Sci 1994, 51, 2165.
10. Reynier,; Dole, A. P.; Humbel, S.; Feigenbaum, A. J Appl Polym Sci 2001, 82, 2422.
11. Reynier, A.; Dole, P.; Feigenbaum, A. J Appl Polym Sci 2001, 82, 2434.
12. Billingham, N. C.; Calvert, P. D. in Developments in Polymer Stabilization, Scott, G., Ed.; Applied Science: London, 1980.
13. Roe, R. J.; Bair, H. E.; Gieniewski, C. J. J Appl Polym Sci 1974, 12, 843.
14. Moisan, J. Y. in Polymer Permeability, Comyn, J., Ed.; Elsevier: London, 1985.
15. Crank, J. G..; Park, S. in Difusion in Polymers Crank, J.; Park, G.. S., Ed.; Academic Press: New York, 1968.
16. Quijada-Garrido, I.; Frutos, G.; Barrales-Rienda, J. M. Macromolecules 1996, 29, 7164.
17. Quijada-Garrido, I.; Barrales-Rienda, J. M.; Alejo Espinoza, L.; Fierro, J. L. G. Macromolecules 1996, 29, 8791.
18. Wakabayashi, M.; Kohno, T.; Kimura, T.; Tamura, S.; Endoh, M.; Ohnishi, S.; Nishioka, T.; Tanaka, Y.; Kanai, T. J Appl Polym Sci 2007, 104, 3751.
19. Wakabayashi, M.; Kohno, T.; Kimura, T.; Tamura, S.; Endoh, M.; Ohnishi, S.; Nishioka, T.; Tanaka, Y.; Kanai, T. 22nd Annual Meeting of the Polymer Processing Society, 2006.
20. Kuwajima, S.; Manabe, A. Chem. Phys. Lett. 2000, 332, 105.
21. Kikuchi, H.; Kuwajima, S.; Fukuda, M. J Chem Phys 2001, 115, 6258.
22. Kuwajima, S.; Kikuchi, H.; Fukuda, M. J Chem Phys 2006, 124, 124111.
23. Fukuda, M.; Kuwajima, S. J Chem Phys 1997, 107, 2149.
24. Fukuda, M.; Kuwajima, S. J Chem Phys 1998, 108, 3001.
25. Nose, S.; J Chem Phys 1984, 81, 511.
26. Hoover, W. G.; Phys Rev 1985, A31, 1695.
27. Andersen H. C.; J Chem Phys 1980, 72, 2384.

28. Linse, P.; Andersen, H.C. J Chem Phys 1986, 85, 3027.
29. Matsuura, T.; Blais, P.; Sourirajan, S. J Appl Polym Sci 1976, 20, 1515.

Captions for Tables and Figures

TABLE I. Parameters obtained from two step transport model

the initial amounts of additives ($C_{0,i}$)
[a] $C_{0,1}$: 15,000ppm, $C_{0,2}$: 17,500ppm, $C_{0,3}$: 20,000ppm
[b] $C_{0,1}$: 4,300ppm, $C_{0,2}$: 6,300ppm

TABLE II. Solubility parameters obtained from molecular dynamics (MD)

TABLE III. Comparison between diffusion coefficients obtained from molecular dynamics (MD) and two step transport model

Figure 1 Concept for calculation of bleeding process assuming the diffusion in the object spread infinitely. (A) t = 0, (B) t = 1/D, (C) t = 4/D.

Figure 2 Internal structure of isotactic polypropylene[19]:
(i) spherulites (S) and amorphous regions (A) among spherulites in iPP film
(ii) internal structure of a spherulite(S)
(iii) the chain folded crystalline regions (C) and amorphous regions (A') among the chain folded crystalline regions.

Figure 3 Bleeding profiles of UVA-1 at 40ºC. Initial amount ($C_{0,i}$) : $C_{0,1}$ = 15,000ppm (■); $C_{0,2}$ = 17,500ppm (▲); $C_{0,3}$ =20,000ppm (●). The full lines are calculated by using the two step transport model.

Figure 4 Bleeding profiles of UVA-2 at 40ºC. Initial amount ($C_{0,i}$) :$C_{0,1}$ = 2,700ppm (■); $C_{0,2}$ = 4,300ppm (▲) ; $C_{0,2}$ = 6,300ppm (●). The full lines are calculated by using the two step transport model.

Figure 5 Final conformation of 50 molecules of UVA-1 per unit cell.
(i) bulk state
(ii) UVA-1 (United Atom model)

Figure 6 Final conformation of 50 molecules of UVA-2 per unit cell.
(i) bulk state
(ii) UVA-2 (United Atom model)

Figure 7 Typical conformation of iPP/UVA-1 blends with 5 chains of iPP (MM:50,000) and 9 molecules of UVA-1 per unit cell.

Figure 8 Typical conformation of iPP/UVA-2 blends with 5 chains of iPP (MM:50,000) and 3 molecules of UVA-2 per unit cell.

Figure 9 Mean square distribution of UV-stabilizers as a function of time; UVA-1: (□, ■); UVA-2: (○, ●). The straight lines shows the least-squares fit by using data from 60 to 200ps.

Figure 10 Comparison of the self diffusion coefficients from MD with the relative diffusion coefficients from two step transport model.

Additive	Temperature ºC	Saturation Solubility *C*s, ppm	Diffusion coefficient *D*, m^2/s	Constant of first-order kinetics *k*, 1/s	Diffusion ratio α_1	α_2	α_3
UVA-1	40ºC	13,000	2.4×10^{-14}	8.1×10^{-7}	0.0[a]	0.0[a]	0.0[a]
UVA-2	40ºC	3,000	7.4×10^{-14}	1.4×10^{-5}	0.11[b]	0.11[b]	

TABLE I

Additive	Potential energy in the vacuum state E_{vac}, kJ/mol	Potential energy in the bulk state E_{bulk}, kJ/mol	Cohesive Energy E_{coh}, kJ/mol	Mole volume V, cm^3/mol	Solubility parameter δ, $MPa^{1/2}$	Saturation solubility from two step transport model C_s, ppm
UVA-1	192	79	113	301	19.3	13,000
UVA-2	129	31	98	189	22.7	3,000
PP	-	-	-	-	17.2[29]	-

TABLE II

Additive	Density by MD d, kg/m^3	Self diffusion coefficients by MD D_{self}, m^2/sec	Relative diffusion coefficients by two step transport model D, m^2/sec
UVA-1	8.3×10^{2}	2.9×10^{-12}	2.4×10^{-14}
UVA-2	8.3×10^{2}	9.1×10^{-12}	7.4×10^{-14}

TABLE III

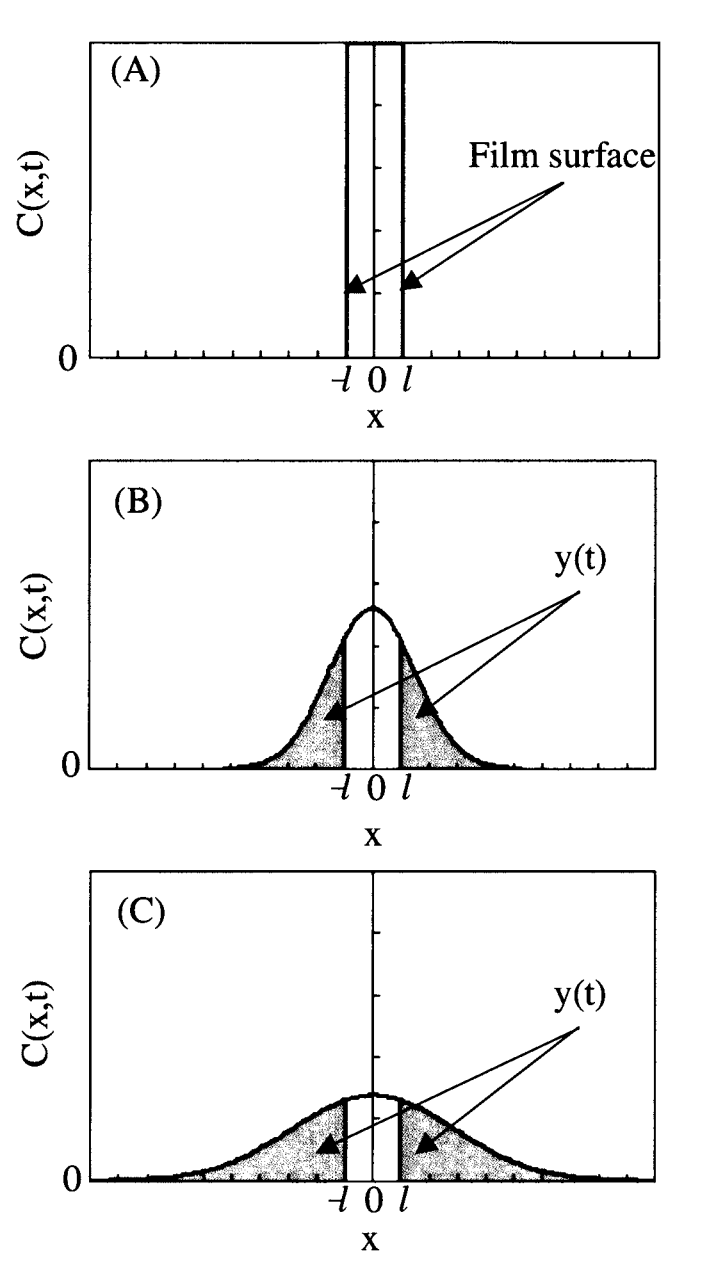
(A)
Film surface
C(x,t)
0
-l 0 l
x
(B)
y(t)
C(x,t)
0
-l 0 l
x
(C)
y(t)
C(x,t)
0
-l 0 l
x

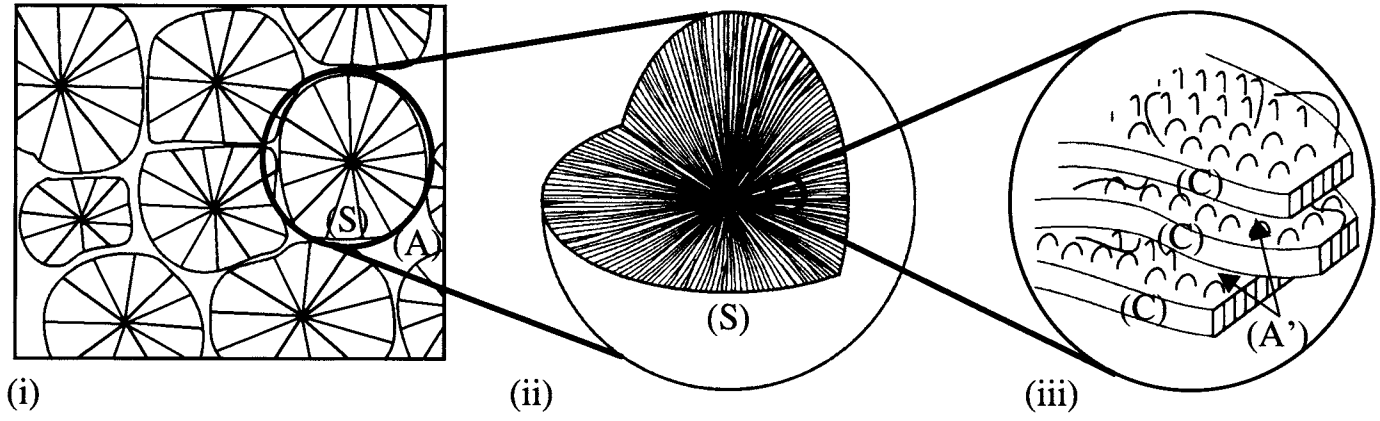
(S)
A
(S)
(C)
(C)
(C)
(A')
(i)
(ii)
(iii)

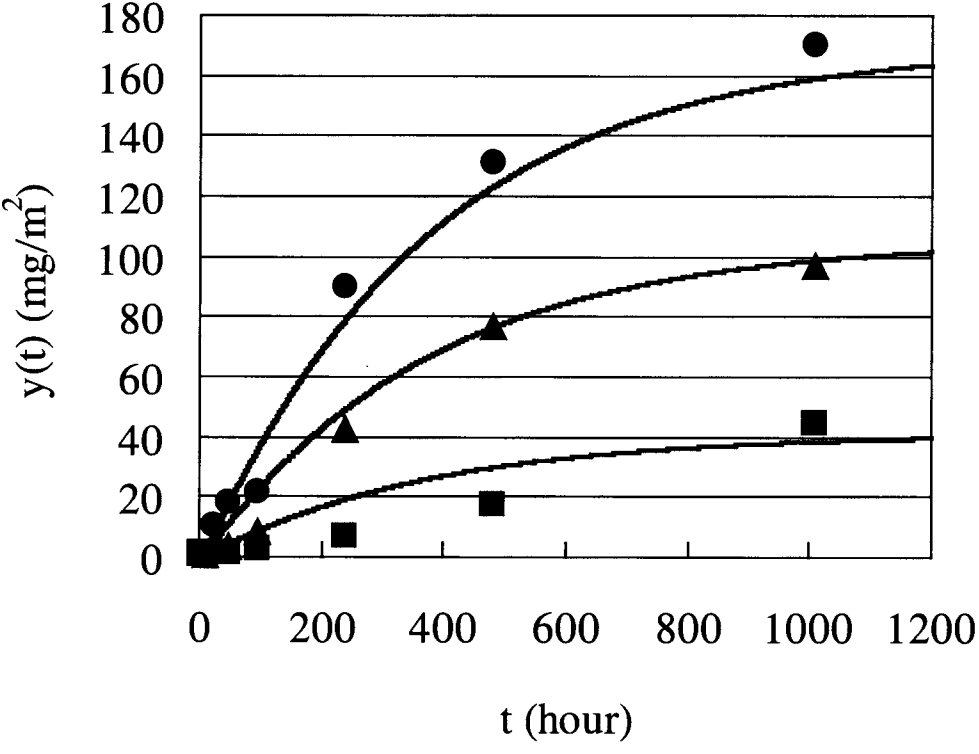
180
160
140
120
100
80
60
40
20
0
y(t) (mg/m2)
0
200
400
600
800
1000
1200
t (hour)

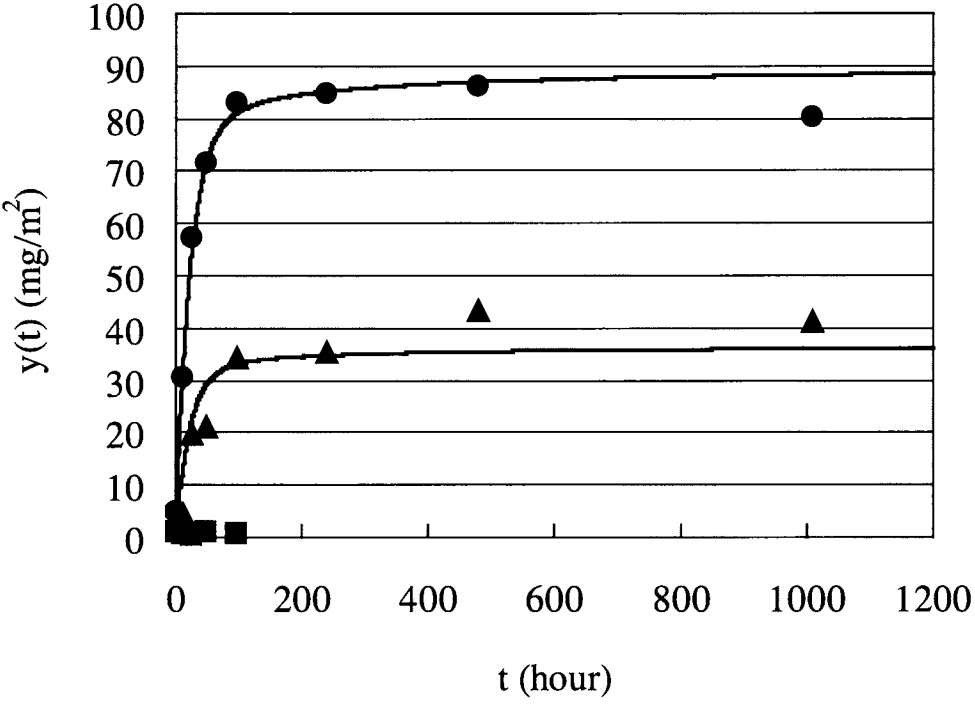
100
90
80
70
60
50
40
30
20
10
0
y(t) (mg/m2)
0
200
400
600
800
1000
1200
t (hour)

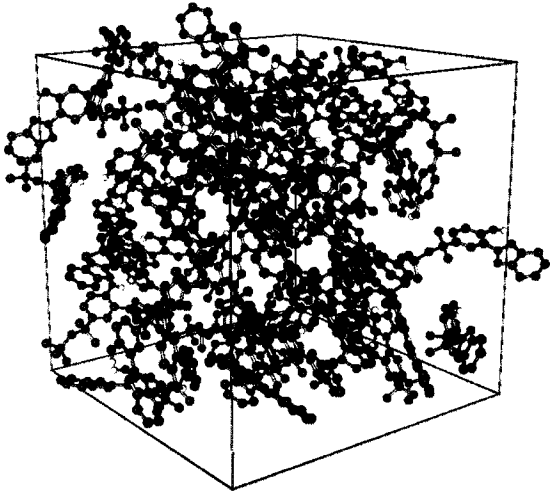

(i)

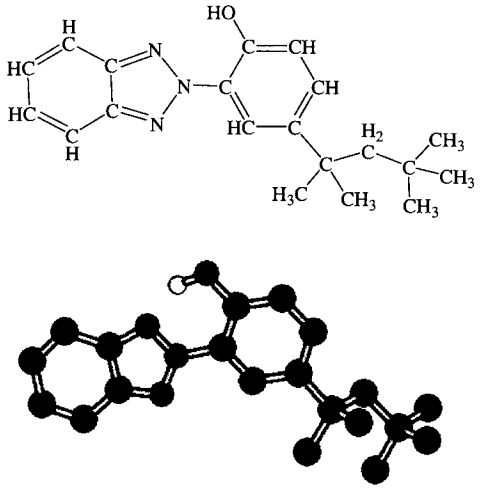

(ii)

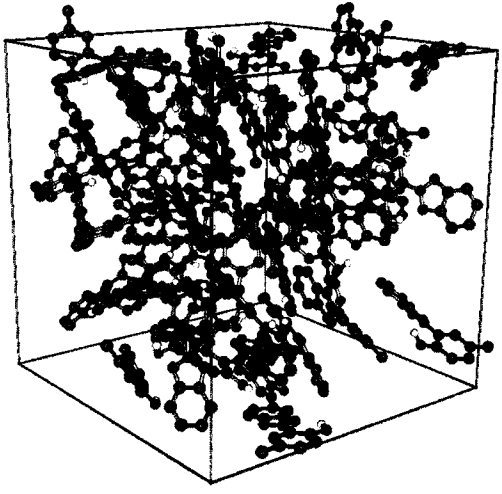

(i)

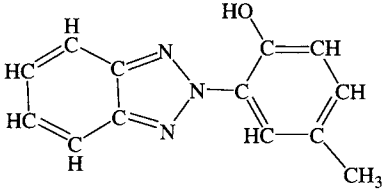

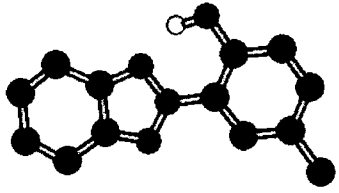

(ii)

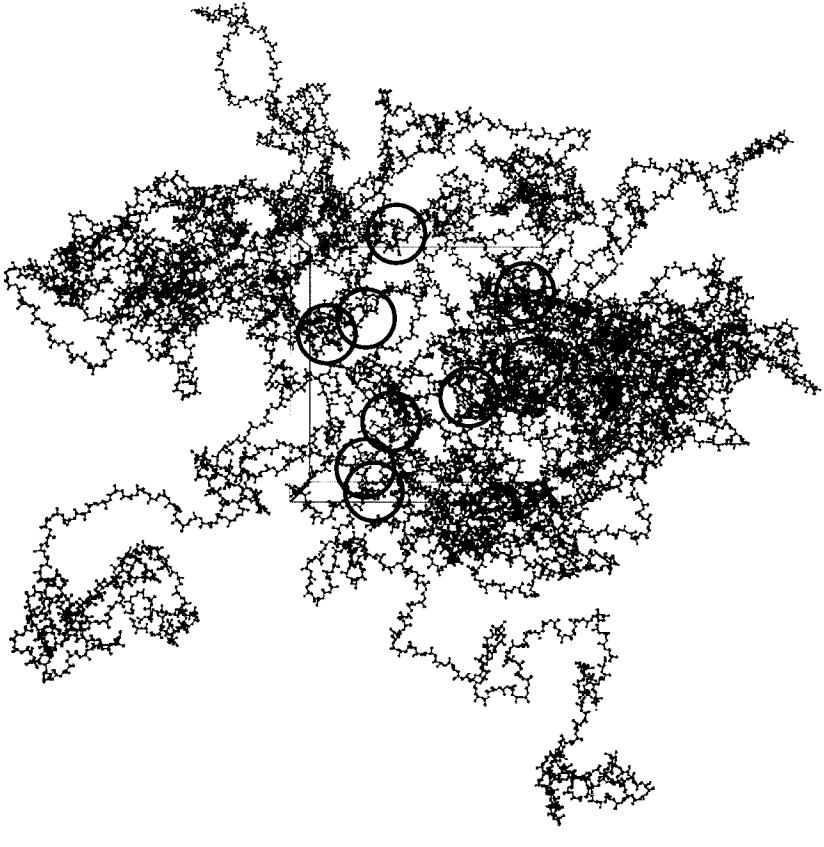

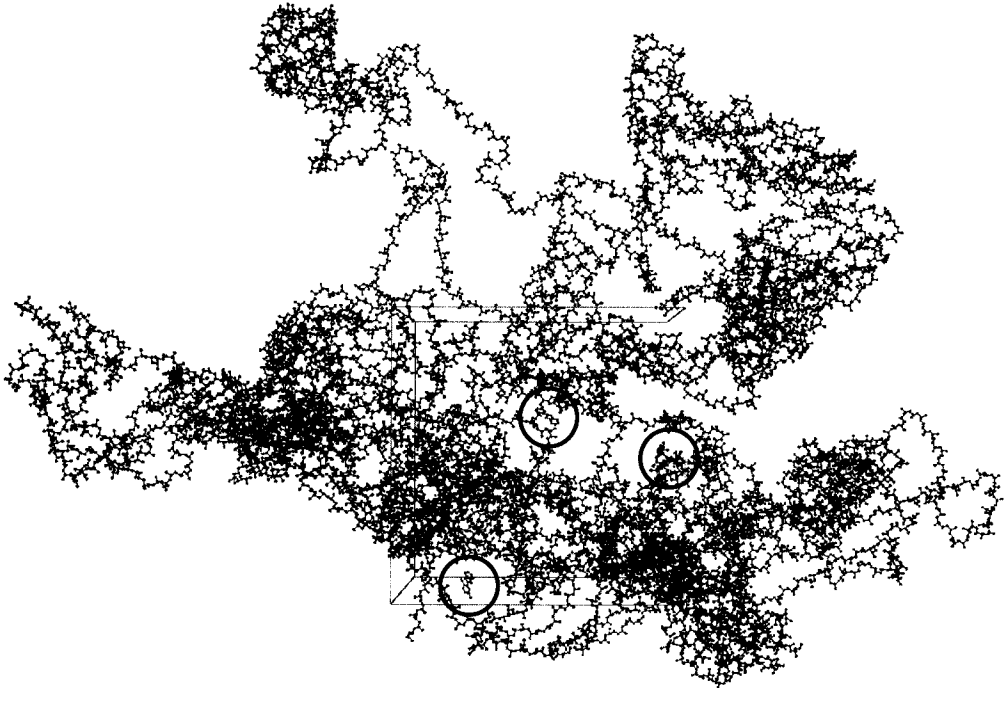

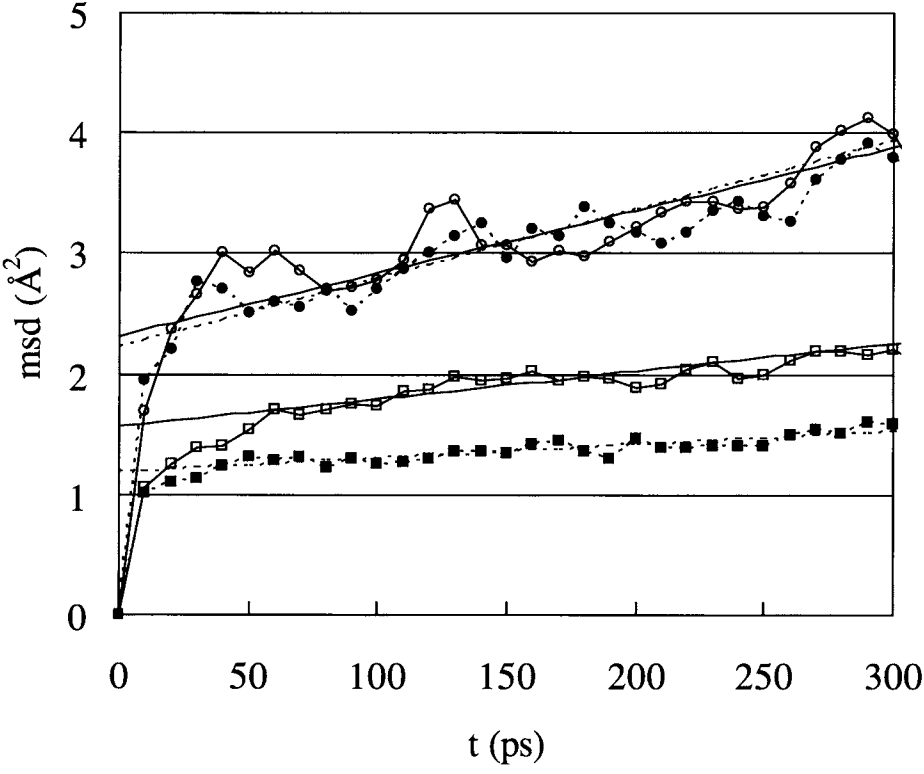
5
4
3
2
1
0
msd (Å^2)
0
50
100
150
200
250
300
t (ps)

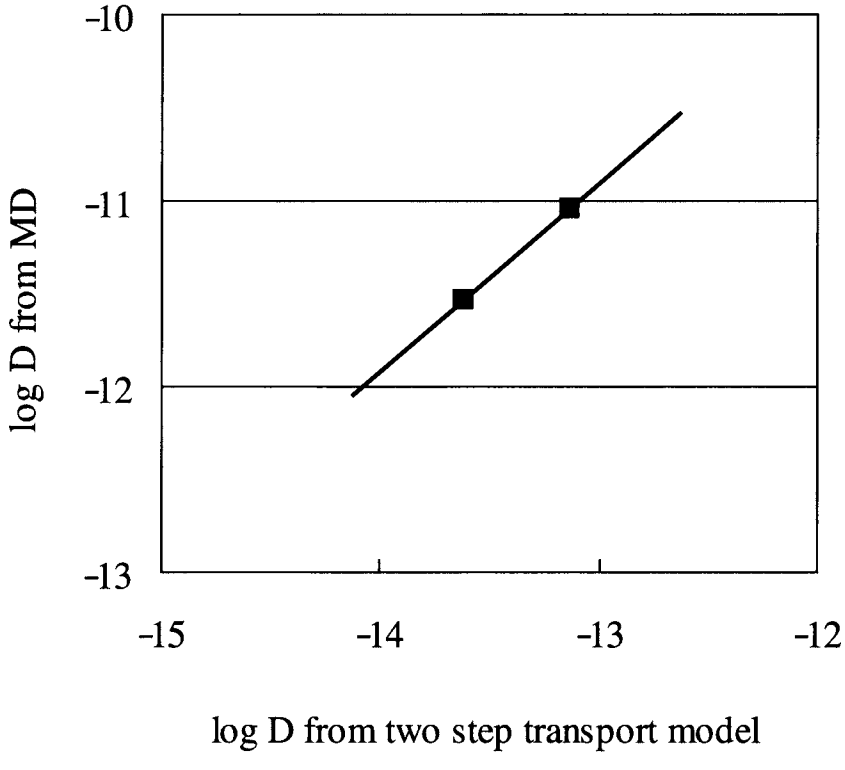
-10
-11
-12
-13
log D from MD
-15
-14
-13
-12
log D from two step transport model